Chinese Chemical Letters 37 (2026) 110576

Contents lists available at ScienceDirect

Chinese Chemical Letters

journal homepage: www.elsevier.com/locate/cclet

ZIF-8 confined carbon dots/bilirubin oxidase on microalgal cells to boost oxygen reduction reaction in photo-biocatalytic fuel cells for pollutants removal

Sili Qing[a], Xuanzhao Lu[a], Yujing Jiang[b], Charitha Thambiliyagodage[d], Bing Song[e], Ao Xia[f,g], Jian-Rong Zhang[a], Wenlei Zhu[b], Li-Ping Jiang[a], Xiaoge Wu[c,*], Jun-Jie Zhu[a,*]

[a] State Key Laboratory of Analytical Chemistry for Life Science, School of Chemistry and Chemical Engineering, Nanjing University, Nanjing 210023, China
[b] State Key Laboratory of Pollution Control and Resource Reuse, School of the Environment, the Frontiers Science Center for Critical Earth Material Cycling, Nanjing University, Nanjing 210023, China
[c] Environment Science and Engineering College, Yangzhou University, Yangzhou 225009, China
[d] Faculty of Humanities and Sciences, Sri Lanka Institute of Information Technology, Malabe, Sri Lanka
[e] Scion, Te Papa Tipu Innovation Park, 49 Sala Street, Private Bag 3020, Rotorua 3046, New Zealand
[f] Key Laboratory of Low-grade Energy Utilization Technologies and Systems, Chongqing University, Ministry of Education, Chongqing 400044, China
[g] Institute of Engineering Thermophysics, School of Energy and Power Engineering, Chongqing University, Chongqing 400044, China

ARTICLE INFO

Article history:
Received 10 September 2024
Revised 4 October 2024
Accepted 22 October 2024
Available online 24 October 2024

Keywords:
Microalgal cells
ZIF-8
Carbon dots
ORR
Photo-biocatalytic fuel cell
Degradation

ABSTRACT

Photocatalytic fuel cells provide promising opportunities for sustainable wastewater treatment and energy conversion. However, their applications are challenged by the sluggish oxygen reducton reaction (ORR) kinetics at cathodes owning to the low O_2 solubility and diffusion rate. Herein, we proposed a photo-biocatalytic fuel cell (PBFC) with a novel hybrid biocathode based on artificially engineered algal cells coated by ZIF-8 confined carbon dots/bilirubin oxidase (ZIF-8/CDs/BOD@algae). Microalgae absorbed CO_2 and provided O_2 *in situ* for BOD catalysts. Due to effective absorption of O_2 by imidazole and confinement of hydrophobic porous ZIF-8, oxygen diffusion has been accelerated in MOF/enzyme systems. Importantly, the introduction of CDs alleviated the poor conductivity of ZIF-8 and improved the electron transfer rate of BOD. Thus, the biocathode exhibited a high current density of 1767 μA/cm^2, a 2.26-fold increase compared with that of CDs/BOD/algae biocathode. Also, it displayed enduring operational stability for up to 60 h since the firmly wrapped ZIF-8 shells could encapsulate proteins and protect algae from the external stimulation. When coupled with Mo:$BiVO_4$ photoanodes, the PBFC exhibited a remarkable power output of 131.8 μW/cm^2 using tetracycline hydrochloride (TCH) as a fuel and an increased degradation rate of TCH. Therefore, this work not only establishs an effective confinement strategy for enzyme to enrich oxygen, but also unveils new possibilities for modified microalgal cells aiding photoelectrocatalytic systems to recover energy from wastewater treatment.

The organic pollutants in wastewater have posed a great threat to human and ecological health [1,2]. Whereas, the development of sustainable water purification systems remains a challenge because harsh reaction conditions and high energy consumption are usually required to remove these refractory contaminants [3–5]. In the past decades, the semiconductor-based photocatalytic fuel cell (PFC) has provided a mild and sustainable approach for wastewater treatment, whilst producing green power [6–8]. The light-induced electrons can spontaneously reach the cathode for ORR, while the photogenerated holes oxidize H_2O/OH^- to generate hydroxyl radicals (•OH) with strong oxidization, facilitating the mineralization of organic matters in wastewater into CO_2 [9]. However, the poor ORR performance at cathodes has limited the development of conventional PFC systems.

On the one hand, because of the low solubility (~8 mg/L) and slow mass transfer (~1.96×10^{-9} m^2/s) of O_2 in H_2O at room temperature and pressure, sluggish ORR kinetics become one of the key limiting factors affecting cell power output, resulting in the unsatisfied degradation efficiency [10,11]. Over the years, substantial efforts have been invested to maximize O_2 mass diffusion. The solid–liquid–air triphasic interface has been constructed since hydrophobic interfaces are believed to improve the O_2 transport

* Corresponding authors.
E-mail addresses: xgwu@yzu.edu.cn (X. Wu), jjzhu@nju.edu.cn (J.-J. Zhu).

https://doi.org/10.1016/j.cclet.2024.110576
1001-8417/

rate [12,13]. Metal-organic frameworks (MOFs) have been proved as useful tools to capture and transfer gas molecules because of their unusually high pore capacity, large specific surface area and tunable capture selectivity [14,15]. Therefore, MOFs have been employed to absorb the dissolved O_2 near the interface from the bulk electrolyte by *in-situ* synthesis of MOF coatings on electrocatalysts, thereby improving ORR performance [11,16].

Alternatively, biological enzymes (*i.e.*, bilirubin oxidase and laccase) exhibit superior ORR catalytic activity with low overpotential at moderate pH values compared with inorganic catalysts [10]. The integrated bio-photoelectrochemical cells composed of photoanodes and enzymatic biocathodes obtained much high energy conversion efficiency [17]. Nevertheless, it is difficult for nature enzymes to be used in harsh conditions because they face activity loss due to the inherent fragility [18]. As a result, we considered developing a MOF/enzyme biocatalyst based on multicopper oxidases with high O_2 confinement effects. This approach holds great promise for addressing the aforementioned issue, given that MOFs can shield enzymes from the deleterious effects of harsh environmental conditions. However, due to the poor conductivity of MOFs, MOF/enzyme systems still face the challenge of poor direct electron transfer (DET) rate. Also, the function and mechanism of oxygen diffusion in MOF/enzyme electrochemical systems have not been fully explored yet. Recently, carbon dots (CDs) have gained significant attention due to their unique electronic and physicochemical properties, including high electron-transfer efficiency, reliable biocompatibility, and photoluminescence [19–22], Consequently, it is a promising way to integrate CDs into MOF/enzyme systems to improve the enzymatic electrocatalytic efficiency.

On the other hand, the energy-intensive aeration process is still needed to guarantee a sufficient O_2 supply, which accounts for over 75 % of the electric energy [23]. Microalgae, as photosynthetic autotrophs, can absorb CO_2 and simultaneously produce oxygen through photosynthesis [24]. In our previous work, we adopted the functionalized algae to *in-situ* supply O_2 to improve the ORR performance in enzymatic biofuel cells even though it suffered from poor operational stability [25]. Furthermore, microalgae have been revived for removing antibiotics in recent years [26]. Nevertheless, the degradation efficiency remained inadequate despite the integration of microalgae with photocatalysts in a homogeneous reaction, because bare microalgae were vulnerable to excessive free radical damage nearby [27].

In this proof-of-concept study, we designed a novel hybrid biocathode based on artificially engineered microalgal cells with O_2 confinement effects as an *in-situ* source of oxygen to increase oxygen mass diffusion and ORR kinetics. The ZIF-8/CDs/BOD@algae was fabricated by biomimetic mineralization. Electrochemical tests and density functional theory (DFT) calculations revealed that owing to the absorption and confinement of O_2 molecules by imidazole, the hydrophobic porous ZIF-8 accelerated oxygen mass diffusion and ORR kinetics. Thus, the biocathode achieved a high current density of 1767 μA/cm^2, which was 2.26 times higher than that of CDs/BOD/algae biocathode. This purposely prepared biocathode showed good electrochemical stability, maintaining 82.4 % of its initial average current density within 60 h. In order to improve the degradation rate of TCH and energy recovery of PBFC, the hybrid biocathode was integrated with Mo:$BiVO_4$/FTO anodes to construct a PBFC in a single compartment without mechanical aeration. The performance of electricity generation and low-energy consumption degradation in PBFC systems were improved. Hence, this work provides the feasibility to expand the application of enzyme and microalgae biocathodes in photoelectrochemical systems for energy-efficient water remediation.

ZIF-8/CDs/BOD coated algal cells were prepared by biomimetic mineralization (Fig. 1a) [28], in which living cells were dispersed in the zinc acetate solution, and then CDs/BOD hybrids and 2-methylimidazole (HMIM) aqueous solutions were added in sequence. After several minutes, the cells were collected from solutions and washed with water. The CDs/BOD hybrids have been characterized in our previous research [25]. The morphology of algal cells before and after ZIF-8/CDs/BOD coating was observed using scanning electron microscopy (SEM) and transmission electron microscopy (TEM) (Figs. 1b-e). Compared with the smooth surface of native cells (Figs. 1b and c), the membrane of modified algal cells was covered with a uniform and rough polycrystalline ZIF-8 shell (Figs. 1d and e), which was consistent with the morphology of ZIF-8/CDs/BOD biocomposites (Fig. S1 in Supporting information). We hypothesized that the biomolecule-rich cell membranes and walls could concentrate MOFs precursors, and provide an effective interface for the crystallization of MOFs [29,30]. Simultaneously, the CDs/BOD biohybrids could be embedded in the framework of ZIF-8 during the nucleation process [31]. Confocal laser scanning microscope (CLSM) was used to reveal the process of biomineralization (Fig. 1f). CDs/BOD hybrids were labeled with fluorescein isothiocyanate (FITC) fluorophore, which produced continuous green fluorescence around each cell. Besides, when doping ZIF-8 nanoparticles with the Rhodamine B (RhB), the blue fluorescence outer layer was overlapped with the green layer, indicating that the CDs/BOD hybrids were encapsulated in the inorganic exoskeleton, suggesting successful generation of the ZIF-8/CDs/BOD layer. After coating, ζ-potential of ZIF-8/CDs/BOD@algae shifted to −16.7 mV compared with that of −24.9 mV for the native cells (Fig. S2 in Supporting information). Also, the dynamic light scattering (DLS) of native algae changed from 2.9 μm to 4.9 μm (Fig. 1g). Notably, the fabrication process had a negligible impact on the viability of the coated cells, with 85.9 % of the coated cells remaining active compared with the 95.7 % activity observed in native cells (Fig. 1h and Fig. S3 in Supporting information).

Fourier transform infrared spectroscopy (FT-IR) was used to explore the biomimetic mineralization reaction (Fig. 1i and Fig. S4 in Supporting information). The spectrum of CDs/BOD showed a distinct absorbance peak at 1647 cm^{-1}, which was caused by the C=O stretching vibration from the amide I band of BOD [32]. After being fixed in ZIF-8/CDs/BOD and ZIF-8/CDs/BOD@algae, it shifted to a higher wave number of 1654 cm^{-1}. This indicated that the protein interacted with the ZIF-8 while the carbonyl of the protein coordinated with the Zn^{2+} nodes of ZIF-8 [33]. X-ray powder diffraction (XRD) patterns showed the crystalline structure of the ZIF-8/CDs/BOD@algae and ZIF-8/CDs/BOD was consistent with the pure sodalite crystalline phase of ZIF-8 (Fig. 1j) [30]. Compared with the pure CDs (2.9 cm^2/g), The Brunauer-Emmett-Teller (BET) specific surface area of ZIF-8/CDs/BOD increased to 37.3 cm^2/g due to the high specific surface area of ZIF-8 (Fig. 1k and Fig. S5 in Supporting information) [34]. The isotherm curve for the ZIF-8/CDs/BOD indicated the presence of micropores and mesopores in the material [35,36]. Thus, the hierarchical pore characteristics were shown in ZIF-8/CDs/BOD with an average pore size of 11.7 nm.

It is well-known that ORR prefers to occur at the solid–liquid–air triphasic interface, where oxygen can diffuse directly to the reaction center from the air phase through the nanostructured hydrophobic substrate with higher O_2 transport rate [13]. Therefore, the surface hydrophobicity was measured by a standard water contact angle test (Fig. 1l). The synthesized pure ZIF-8 had super-hydrophobicity with a water contact angle of 161.2°. When the ZIF-8 particles mineralized on the surface of algal cells (ZIF-8@algae), the water contact angle changed to 117.8° from the native algae of 83°. It is worth noting that the ZIF-8/CDs/BOD@algae had a super-hydrophilic surface (0°). The phenomenon was identified further by the TEM images (Fig. S6 in Supporting information) that during the nucleation of ZIF-8, some of the hydrophilic CDs were derived outside the ZIF-8 structure, while the internal cavity of ZIF-8 was still hydrophobic, which gave rise to a hydrophilic

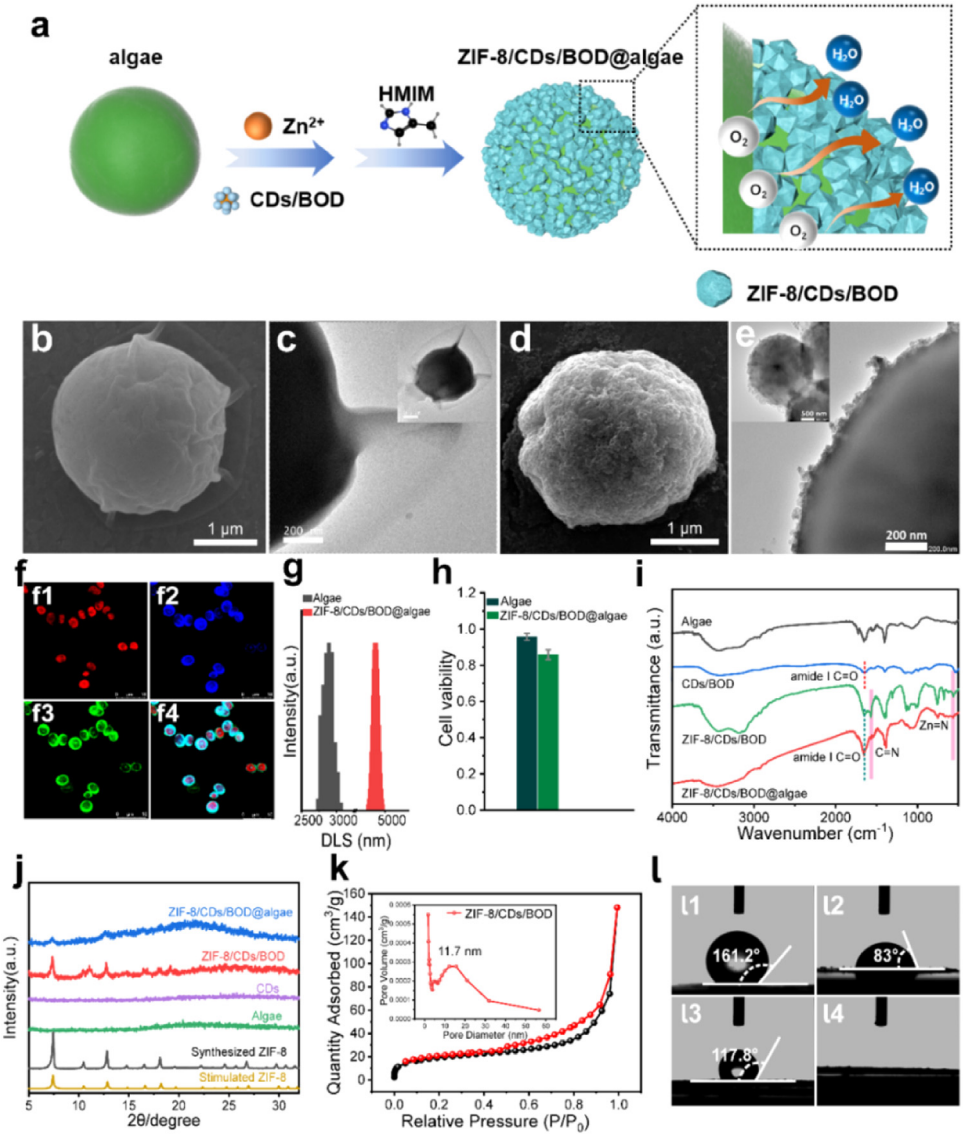

Fig. 1. Fabrication and characteristics of ZIF-8/CDs/BOD@algae. (a) Schematic illustration showing the biomimetic mineralization of ZIF-8/CDs/BOD coated on the algal cell. (b) SEM and (c) TEM images of localized regions and whole cells (insets) of the native algal cells. Scale bar: 500 nm (Inset). (d) SEM and (e) TEM images of localized regions and whole cells (insets) of the ZIF-8/CDs/BOD@algae. Scale bar: 500 nm (Inset). (f) CLSM images of the ZIF-8/CDs/BOD@algae displayed in (f1) red, (f2) blue, (f3) green channels and (f4) overlay images. Red fluorescence, intracellular chlorophyll; blue, RhB labeled MOF shell; green, FITC labeled CDs/BOD hybrids. Scale bar: 10 μm. (g) DLS tests of native cells and ZIF-8/CDs/BOD@algae. (h) The cell viability measurement of native algal cells and ZIF-8/CDs/BOD coated cells. (i) FT-IR of native algae, CDs/BOD hybrids, ZIF-8/CDs/BOD and ZIF-8/CDs/BOD@algae. (j) XRD of stimulated ZIF-8, synthesized ZIF-8, native cells, CDs, ZIF-8/CDs/BOD and ZIF-8/CDs/BOD@algae. (k) The N_2 sorption isotherms and pore width (Inset) of ZIF-8/CDs/BOD. (l) The water contact angles of (l1) ZIF-8, (l2) native algae, (l3) ZIF-8@algae and (l4) ZIF-8/CDs/BOD@algae.

contact angle for ZIF-8/CDs/BOD@algae [33]. The appropriate hydrophobic/hydrophilic interface and porous structure are beneficial for both H_2O discharge and O_2 transport.

The electrocatalytic ORR performance of biocathodes was investigated by linear sweep voltammetry (LSV) and the illustration of ORR occurred at the liquid-solid-air interface was shown in Fig. 2a. Firstly, the mass ratio of BOD, CDs, and the precursor concentration (HMIM and Zn^{2+} ion) were optimized (Fig. S7 in Supporting information). The optimized conditions involved 20 μL BOD, 75 μg CDs and 100 μL ligand precursors. To study the influence of the ZIF-8 and CDs on the ORR performance of algal biocathodes, the current density was measured by LSV tests after 5 h illumination. As shown in Fig. 2b, the current density of ZIF-8/CDs/BOD@algae biocathode reached the highest current density of 1767 μA/cm^2 at 0.3 V, which was 2.26 times, 4.28 times and 5.08 times higher than that of CDs/BOD/algae (781.8 μA/cm^2), BOD/algae (413.2 μA/cm^2) and ZIF-8/BOD/algae (347.8 μA/cm^2) biocathodes, respectively. Compared with previous studies, the enzyme/algae biocathode has competitive performance in bilirubin oxidase biocatalysts, in which the amount of drop casting enzymes is much less (Table S1 in Supporting information). Besides, the formal potential of the ZIF-8/CDs/BOD@algae was tested to be 0.472 V (*vs.* SCE), which was more positive than that of CDs/BOD/algae (0.456 V *vs.* SCE). These favourable enhancements could be ascribed to the conductivity of CDs and the confinement of ZIF-8 framework. The electrochemical impedance spectroscopy (EIS) (Fig. S8 in Supporting information) showed that with the addition of CDs, the charge transfer resistance (R_{ct}) of ZIF-8/CDs/BOD@algae decreased significantly compared with ZIF-8/CDs/algae. Furthermore, the reduced overpotential indicated that the ZIF-8 could promote the DET rate of enzymes by shortening the distance between BOD and CDs, which was consistent with the previous report [37].

In order to prove the importance of *in-situ* produced O_2, we studied the difference of O_2 supply modes between the self-

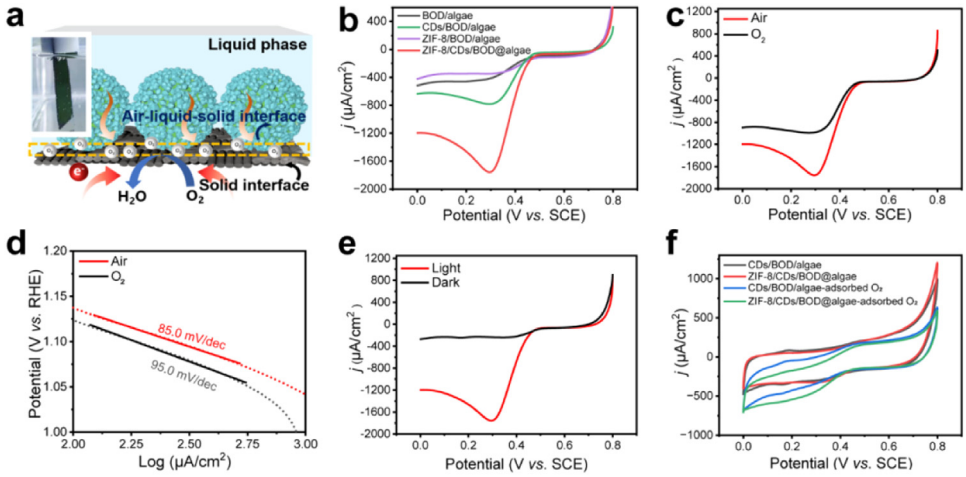

Fig. 2. (a) The illustration of ZIF-8/CDs/BOD@algae biocathode for *in-situ* O_2 supply at the triphasic interface and the corresponding photograph (Inset). (b) LSV curves of different electrodes. (c) LSV curves of ZIF-8/CDs/BOD@algae in O_2 saturated solutions under dark conditions (black) and in air atmosphere under light conditions (red), scan rate: 10 mV/s. (d) The corresponding Tafel plots. (e) LSV curves of the ZIF-8/CDs/BOD@algae electrode under the light illumination (red) and dark conditions (black). (f) CVs of ZIF-8/CDs/BOD@algae and CDs/BOD/algae electrodes in 0.1 mol/L O_2-free PBS solutions (pH 7.0), scan rate: 10 mV/s.

supplied O_2 through photosynthesis (Fig. 2a) and supplied O_2 through conventional simple O_2 diffusion approach, in which O_2 diffuses from the bulk solution to the reaction interface driven by a concentration gradient. The ZIF-8/CDs/BOD@algae biocathode with *in-situ* produced O_2 had a higher current density (Fig. 2c) and smaller Tafel slope than conventional O_2 diffusion (Fig. 2d), indicating that the *in-situ* supplied O_2 of ZIF-8/CDs/BOD@algae had faster ORR reaction kinetics [38]. Due to the sustainable produced O_2 *via* photosynthesis, the current density of ZIF-8/CDs/BOD@algae was almost 7.4 times higher under illumination than that under dark conditions (Fig. 2e).

It has been reported that ZIF-8 exhibits the capability to store oxygen [16]. The role of ZIF-8 in O_2 diffusion in MOF/enzyme/algae systems was explored *via* cyclic voltammetry (CV) measurements. The biocathode was pretreated for 30 min under illumination to produce O_2 *in-situ via* photosynthesis and then moved into O_2-free PBS solutions, followed by CV tests (Fig. 2f). It demonstrated that the peak current of ZIF-8/CDs/BOD@algae was higher than that of CDs/BOD/algae biocathode, suggesting that the ZIF-8 coating could enrich and transfer the O_2 to the BOD catalyst directly without diffusing to the bulk electrolyte and further enhance the ORR performance. O_2 enrichment in the porous ZIF-8 was interpreted to accelerate the local O_2 diffusion due to a higher concentration gradient [11]. To estimate the oxygen diffusion coefficient (D_{O_2}), a diffusion-limited peak current (i_p) was measured under different scan rates (ν). The peak current was dictated by the mass diffusion coefficient as Randle-Sevcik equation (Text S15 in Supporting information) [39],

$$i_p = Bn^{2/3}AD^{1/2}C\nu^{1/2} \quad (1)$$

As the equation was associated with the electrochemical active surface area (ECSA) of biocathodes, which was estimated by the double-layered capacitance (C_{dl}) according to the equation in Text S14 (Supporting information) [40]. As calculated, the CDs/BOD/algae and ZIF-8/CDs/BOD@algae biocathodes had almost the same value of C_{dl}, indicating that the ORR performance has little relationship with the ECSA (Fig. S9 in Supporting information). As shown in Fig. S10 (Supporting information), the growth of i_p slowed down with the increase of ν in the diffusion-control potential region, and the value of D_{O_2} inside ZIF-8/CDs/BOD@algae biocathodes was calculated to be about 3.98×10^{-5} cm^2/s, which was higher than that of CDs/BOD/algae (2.04×10^{-5} cm^2/s), even higher than the D_{O_2} in 0.1 mol/L KOH solutions ($D_{O_2} = 1.9 \times 10^{-5}$ cm^2/s) [41]. It can be concluded that the ZIF-8 coating can greatly improve the oxygen diffusion rate, because of its excellent ability to enrich and transfer O_2 through the hydrophobic ZIF-8 pores. As a result, this leads to a substantial improvement in the ORR kinetics [15,39].

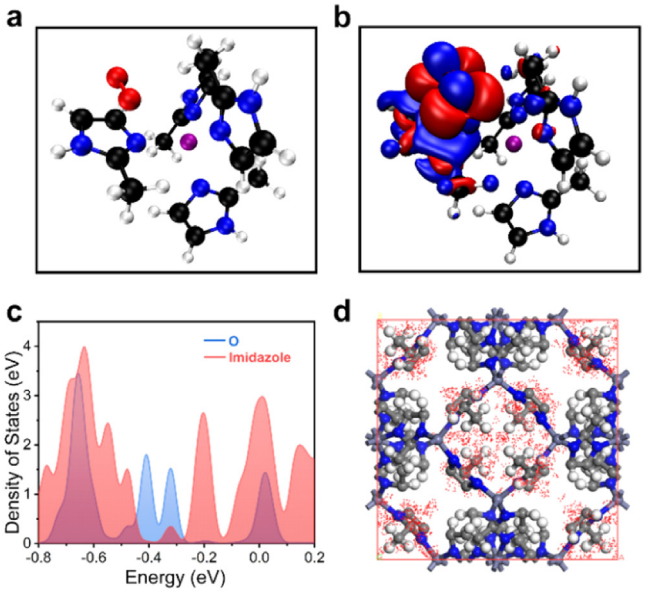

Fig. 3. (a) The DFT calculations of optimized geometries of ZIF-8/O_2. (b) Charge density differences for O_2 adsorption. (c) DOS for O atoms adsorbed on imidazole of ZIF-8. (d) The COM probability density distributions for O_2 adsorbed on imidazole of ZIF-8.

DFT calculations were utilized to study the microscopic interactions between concentrated O_2 and ZIF-8 (Text S16 in Supporting information). Initially, the optimized geometries of ZIF-8/O_2 was elucidated in Fig. 3a. The result showed that ZIF-8 exhibited moderate binding affinities towards oxygen molecules (binding energy, $E_b = -0.51$ eV), a level of interaction not excessively robust to impede the efficient utilization of oxygen by the BOD [42]. Furthermore, the independent gradient model based on Hirshfeld partition (IGMH) analysis (Fig. S11 in Supporting information) revealed a notable non-covalent interaction between oxygen molecules and 2-methylimidazole, thus confirming the suitable adsorption binding

energy between ZIF-8 and O_2 [43]. The charge density difference (CDD) between the absorbed O_2 molecules and the ZIF-8 was analysed (Fig. 3b). After adsorption, there was a notable charge transfer between O_2 molecules and ZIF-8 structure, with electrons migrating from imidazole to O_2, illustrating the efficient enrichment of O_2 by ZIF-8 while facilitating its subsequent reduction. Likewise, the interactions between the imidazole of ZIF-8 and O_2 molecules were examined through an electronic density of states (DOS) analysis (Fig. 3c and Fig. S12 in Supporting information) [44]. A substantial overlap between the C-p states and O-p states was observed within the imidazole framework [45]. Additionally, the center-of-mass (COM) probability distribution (Fig. 3d) for the O_2 molecules within the ZIF-8 structures clearly indicated an enhanced density distribution, suggesting a propensity for O_2 adsorption. These findings confirm that the imidazole groups in the porous ZIF-8 structure absorb and enrich O_2 molecules, thereby accelerating oxygen mass diffusion and boosting the ORR kinetics.

Additionally, the long-term operation stability of electrodes was continuously monitored by the constant potential *i-t* curves under the 12-h light/12-h dark cycle (Fig. S13 in Supporting information). The ZIF-8/CDs/BOD@algae exhibited good electrochemical stability within 60 h, maintaining 97 % and 82.4 % of its initial average current density during the second and the third cycles, respectively, while the CDs/BOD/algae only maintained 72 % of its initial performance during the third cycles. Besides, the ORR current density was more than double that of the CDs/BOD/algae. Furthermore, the cell viability after a 12-h ORR test was assessed by CLSM analysis (Fig. S14 in Supporting information). The CDs/BOD/algae showed more red fluorescence with a low survival rate (69 %), in contrast to a high cell viability for the ZIF-8/CDs/BOD@algae (86.8 %), indicating that ZIF-8 had a protective effect on algae. In addition, when the biocathodes were explored in the electrolyte containing 10 mg/L TCH, the ZIF-8/CDs/BOD@algae showed a 90 % survival rate, markedly higher than CDs/BOD/algae biocathodes (52.3 %) (Fig. S15 in Supporting information). Notably, for the ZIF-8/CDs/BOD system, the ZIF-8 shell helped retain 63.3 % of its original current density in the DMSO solution. On the contrary, the current density of CDs/BOD dropped significantly to 5.9 % of its original performance (Fig. S16 in Supporting information). This is consistent with the previous reports that the MOFs helped maintain the enzyme's structure to prolong enzyme stability [37]. To sum up, the ZIF-8 coating serves not only to shield the algal cells from adverse environmental conditions, including electronic and antibiotic influences, but also enhance enzyme's stability, thereby advancing the electrochemical stability of ZIF-8/CDs/BOD@algae.

The Mo:$BiVO_4$/FTO photoanode was prepared by a simple spin-coating method with modification (Fig. S17 in Supporting information) [46]. SEM images of Mo:$BiVO_4$ (Figs. S17a and b) showed a worm-like and uniformly stacked porous structure with a thickness of about 700 nm. XRD patterns (Fig. S17c) demonstrated that Mo:$BiVO_4$ was the phase-pure monoclinic $BiVO_4$ (JCPDS No. 13-0688). According to the corresponding UV–visible diffuse reflectance spectra (Fig. S17d) and Tauc plot (Fig. S17e), the corresponding band gap (E_g) was estimated to be 2.63 eV (Text S17 in Supporting information) [47]. The valence band edge (E_{VB}) of Mo:$BiVO_4$ was determined to be about 2.18 eV by X-ray photoelectron spectroscopy (XPS). Therefore the conduction band edge (E_{CB}) was estimated to be about −0.45 eV due to $E_{VB} = E_g + E_{CB}$ (Fig. S17f) [48]. LSV tests were carried out under visible light irradiation to investigate the photoelectrochemical properties of photoanodes toward water oxidation reaction (WOR) (Fig. S18a in Supporting information). We observed that doping metal dopants (Mo^{6+}) significantly improved the electron transport efficiency of bismuth vanadate and reached a high current density of 2.3 mA/cm^2 after a three-times of spin coating at 1.23 V (*vs.* RHE) (Fig. S18b in Supporting information). In addition, the Mo:$BiVO_4$ photoanode exhibited a onset potential of 0.1 V (*vs.* RHE), a negative shift was observed compared with 0.15 V of pure $BiVO_4$. This might be attributed to the reduction of Fermi level pinning by Mo^{6+} modification, as previously reported [17].

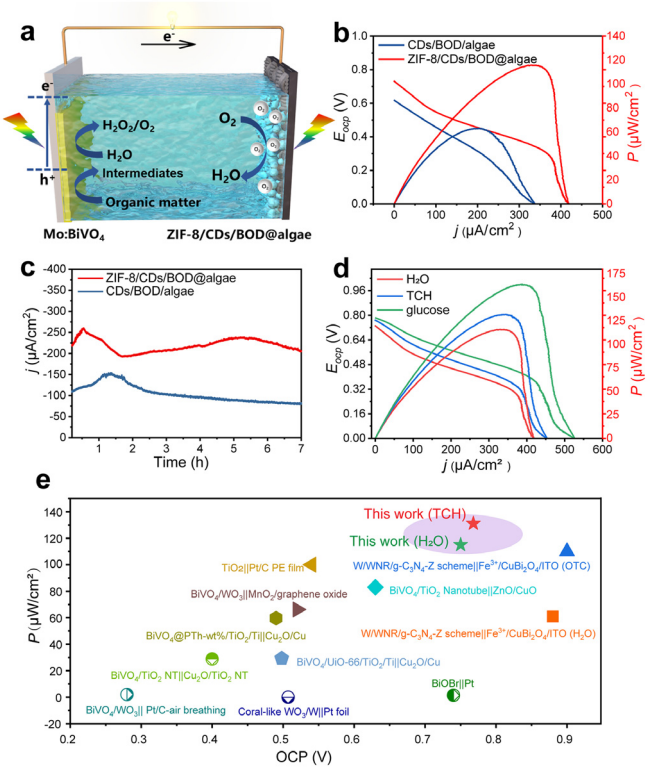

Fig. 4. (a) The schematic illustration of PBFC based on ZIF-8/CDs/BOD@algae biocathodes. (b) Polarization curves (*J-V*) and power density (*J-P*) curves of the PBFC and (c) the long-term operational stability in PBS solutions (pH 7.0). (d) *J-V* and *J-P* curves of ZIF-8/CDs/BOD@algae based PBFC in different fuels. (e) Comparison of the performance metrics of PBFC based on Mo:$BiVO_4$ photoanodes and ZIF-8/CDs/BOD@algae biocathodes with other PFCs.

The ZIF-8/CDs/BOD@algae biocathode was then integrated with the Mo:$BiVO_4$/FTO photoanode to fabricate a PBFC as shown in Fig. 4a. The power generation performance of the PBFC was measured by LSV measurements and the polarization curves (*J-V*) and power density (*J-P*) plots were shown in Fig. 4b. The open-circuit potential (OCP) of PBFC based on ZIF-8/CDs/BOD@algae in water was 0.73 V, with a maximum power density (P_{max}) of 115.8 μW/cm^2, which was much higher than that of CDs/BOD/algae based PBFC (63.0 μW/cm^2). Fig. 4c showed the stability of PBFC systems in long-term operation. As illustrated, the ZIF-8/CDs/BOD@algae based PBFC maintained 93 % of its initial short-circuit current within 7 h, whereas the CDs/BOD/algae based PBFC kept only 73 % of its initial short-circuit current. This result was consistent with the stability of a single cathode discussed above. In addition, a series of typical organic molecules in wastewater were selected as the fuel to obtain the *J-V* and *J-P* plots, so as to further investigate the PBFC performance based on ZIF-8/CDs/BOD@aglae biocathodes. As shown in Fig. 4d, the OCP value in the presence of glucose was the highest (0.78 V), followed by the TCH (0.77 V), both of which were higher than that of H_2O (0.73 V). Glucose as fuels exhibited the highest power output of 163.8 μW/cm^2. Notably, compared with H_2O, TCH as a fuel had a higher power output (131.8 μW/cm^2), suggesting that the high oxidation capacity of PBFC could be used to directly oxidize the TCH to generate electricity. Nevertheless, due to the absorption of visible light by RhB, the power density was 100 μW/cm^2, slightly lower than that of H_2O (Fig. S19 in Sup-

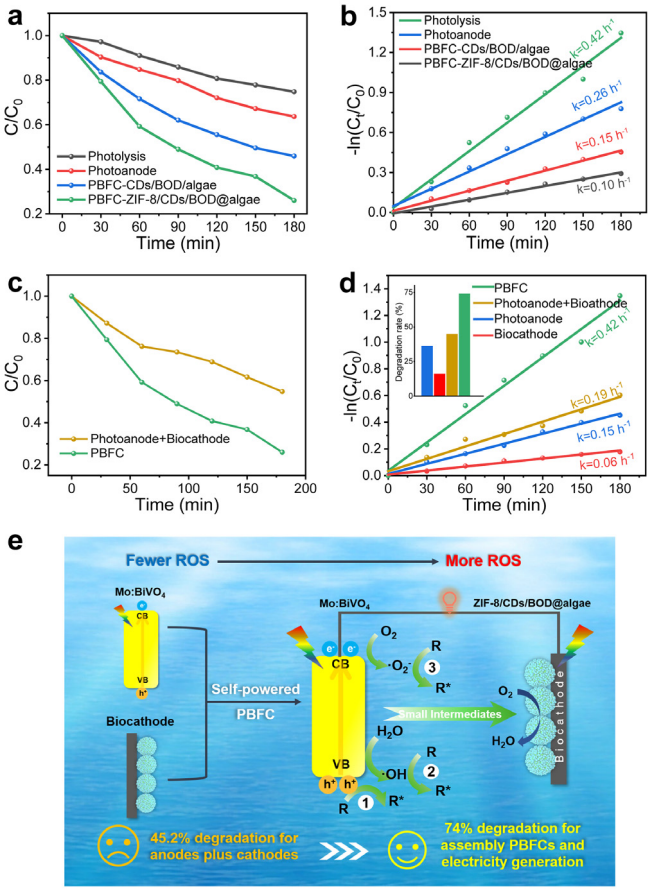

Fig. 5. (a) TCH degradation in different systems and (b) the corresponding reaction kinetic plots. Experiments were conducted under short-circuit conditions in 0.1 mol/L PBS solution (pH 7) with 10 mg/L of TCH. (c) The remove efficiency of TCH by the PBFC-ZIF-8/CDs/BOD@algae under the open-circuit conditions (Photoanode+Biocathode) or short-circuit conditions. (d) The reaction kinetic plots of different components for TCH degradation. Inset, the corresponding degradation rate. (e) The schematic illustration of the PBFC to remove organic pollutants.

porting information). Therefore, the PBFC performance in electricity generation has remarkable superiorities compared with other PFC systems based on ORR cathodes (Fig. 4e and Table S2 in Supporting information). Afterwards, the 10 mg/L of TCH was chosen as the optimistic value for further degradation experiments considering the power density (Fig. S20 in Supporting information) and the toxicity to algal cells.

As indicated above, PBFC has the potential to eliminate pollutants, given its large short-circuit currents and strong oxidation ability. This capability was evaluated by the degradation of RhB and TCH in an aqueous solution when the adsorption-desorption equilibrium was reached within 20 min and the results were exhibited in Table S3 (Supporting information). For the degradation of RhB (Fig. S21a in Supporting information), the PBFC based on the ZIF-8/CDs/BOD@algae showed the highest degradation rate, reaching 96.2 % within 2 h, higher than that of PBFC based on CDs/BOD/algae (54.8 %) and the photocatalytic degradation by photoanodes (39.5 %).

To quantitatively analyze the degradation process, *pseudo* first-order kinetics was used to simulate the degradation curves. It can be observed that the PBFC based on the ZIF-8/CDs/BOD@algae exhibited the largest rate constant (k) of 0.0298 min^{-1} compared with other counterparts (Fig. S21b in Supporting information). For the degradation of TCH (Figs. 5a and b), based on ZIF-8/CDs/BOD@algae, the PBFC removed 74.0 % of TCH within 3 h, while based on CDs/BOD/algae electrodes, the removal efficiency of the PBFC was only 54.1 %, followed by the photoanode degradation (36.3 %). The ZIF-8/CDs/BOD@algae based PBFC had a rate constant of 0.42 h^{-1}, which was 1.64 times and 2.8 times higher than that of CDs/BOD/algae based PBFC and photoanodes system, respectively. The above results suggested that PBFC based on ZIF-8/CDs/BOD@algae system possessed the highest degradation efficiency. The PBFC performance also showed clear superiorities in the degradation of RhB and TCH compared to the previous researches (Tables S4 and S5 in Supporting information) considering the low energy input and economic cost, whilst an additional aeration process is not required.

This excellent purifying performance can be attributed to the fast charge separation of Mo:$BiVO_4$ photoanodes promoted by the outstanding ZIF-8/CDs/BOD@algae biocathodes. Furthermore, the degradation was tested under an open-circuit condition where no currents passed through an external circuit (hereafter, Photoanode+Biocathode) (Fig. 5c). Only about 45.2 % of TCH removal was observed, indicating that short-circuit current had a significant influence on removal rate. In addition, the single photoanode and biocathode exhibited 36.3 % and 16.1 % of degradation rate, respectively, with much lower rate constant as shown in Fig. 5d. This indicates that the PBFC's degradation performance is markedly enhanced with the integration of biocathodes. It can be inferred that enhanced ORR performance tends to increase the charge separation of the photoanode, and thus increase the production of reactive oxidative species (ROS). In order to explore the existence of the free radicals, the electron paramagnetic resonance (EPR) spectra was employed under illumination. As shown in Fig. S22 (Supporting information), the signal of TEMPO-h^+, DMPO-$^{\bullet}O_2^-$ and DMPO-$^{\bullet}$OH was observed.

In this work, it is difficult for the sole photocatalytic anode to completely mineralize the persistent organic matrix [49]. Alternatively, the degradation of TCH from the biocathode within a short time was ineffective [50]. However, it is noted that when the photoanode was coupled with the biocathode, the degradation rate was significantly improved. The mechanism is proposed in Fig. 5e. There is a large potential difference between the onset potential of Mo:$BiVO_4$ (0.1 V *vs.* RHE) and the onset potential of ZIF-8/CDs/BOD@algae (1.126 V *vs.* RHE), which drives the charge separation and transfer of photoanodes. It is suggested that under the irradiation of simulated sunlight, the valence band holes oxidate H_2O to H_2O_2 or $^{\bullet}$OH, while the electrons are transferred to the ZIF-8/CDs/BOD@algae biocathode through the external circuit and reduce O_2 to H_2O. Meanwhile, some electrons can also reduce the O_2 to produce $^{\bullet}O_2^-$ at the photoanode [51]. Thus, the h^+, $^{\bullet}$OH and $^{\bullet}O_2^-$can directly react with organic pollutants for degradation in the PBFC system. As a result, it is a promising way to integrate photocatalytic degradation with microalgal biocathodes, where no energy input is needed except the solar source.

In summary, the ORR performance can be greatly improved by constructing a confined catalytic layer on the surface of live microalgal cells. ZIF-8 MOFs were used to successfully mineralize carbon dots/bilirubin oxidase *in situ* on individual microalgal cells, resulting in multifunctional effects encompassing *in-situ* oxygen supply, enzyme immobilization, and accelerated oxygen mass diffusion. Consequently, the biocathode exhibited rapid ORR kinetics and attained a notable current density of 1767 μA/cm^2, 2.26 times higher than the CDs/BOD/algae. Also, the firmly wrapped ZIF-8 shells improved the DET rate of enzymes and protected the microalgae from the antibiotic stimulation, demonstrating a durable operational stability with 82.4 % retention of its initial average current density within 60 h. On this basis, we combined the biocathode and a photoanode to treat model organic pollutants cooperatively. With a Mo:$BiVO_4$ photoanode, the PBFC exhibited a maximum power density of 131.8 μW/cm^2 using TCH as fuels with

an open-circuit potential of 0.77 V under visible light illumination. The degradation efficiency reached 74 % in 3 h, outperformed the simple combination of photoanodes and biocathodes. It can be attributed that the enhanced ORR performance helps separate the photoinduced electron/hole pairs from the Mo:$BiVO_4$ due to the energy bias between the anode and cathode, leaving more holes and $^{\bullet}OH$ oxidating with organic pollutions. Hence, this purposely modified strategy provides a possibility for enzyme and microalgae biocathodes to assist photocatalysts for power generation from dissolved organic pollutants in an energy-efficient way to boost carbon neutralization.

Declaration of competing interest

The authors declare that they have no known competing financial interests or personal relationships that could have appeared to influence the work reported in this paper.

CRediT authorship contribution statement

Sili Qing: Writing – original draft, Investigation, Data curation, Conceptualization. **Xuanzhao Lu:** Writing – review & editing. **Yujing Jiang:** Writing – review & editing. **Charitha Thambiliyagodage:** Writing – review & editing. **Bing Song:** Writing – review & editing. **Ao Xia:** Writing – review & editing. **Jian-Rong Zhang:** Supervision. **Wenlei Zhu:** Writing – review & editing, Supervision, Funding acquisition. **Li-Ping Jiang:** Writing – review & editing, Supervision. **Xiaoge Wu:** Writing – review & editing, Methodology, Conceptualization. **Jun-Jie Zhu:** Writing – review & editing, Project administration, Funding acquisition.

Acknowledgments

The authors would like to acknowledge the support from National Natural Science Foundation of China (Nos. 22176086, 52100014), Natural Science Foundation of Jiangsu Province (No. BK20210189), State Key laboratory of Pollution Control and Resource Reuse, the Fundamental Research Funds for the Central Universities (Nos. 021114380183, 021114380189, 021114380199), the Research Funds from Frontiers Science Center for Critical Earth Material Cycling of Nanjing University, Research Funds for Jiangsu Distinguished Professor, Carbon Peaking and Carbon Neutrality Technological Innovation Foundation of Jiangsu Province (No. BE2022861), the Central Universities - Cemac "GeoX" Interdisciplinary Program (No. 021114380217), Frontiers Science Center for Critical Earth Material Cycling of Nanjing University (No. 2024QNXZ07), Postdoctoral Fellowship Program of CPSF (No. GZC20231105) and the Jiangsu Funding Program for Excellent Postdoctoral Talent (No. 2023ZB226).

Supplementary materials

Supplementary material associated with this article can be found, in the online version, at doi:10.1016/j.cclet.2024.110576.

References

[1] G. Zhang, Y. Li, C. Zhao, et al., Nat. Nanotechnol. 19 (2024) 1130–1140.
[2] W. Zheng, H. Guo, C. Zhu, et al., Energy Environ. Mater. 6 (2023) e12476.
[3] D. Yu, L. Xu, K. Fu, et al., Nat. Commun. 15 (2024) 2241.
[4] Q. Yan, C. Lian, K. Huang, et al., Angew. Chem. Int. Ed. 60 (2021) 17155–17163.
[5] Y. Jiang, S. Tian, H. Li, et al., TIMS 1 (2023) 100008–100014.
[6] C. Dong, Y. Yang, X. Hu, et al., Nat. Commun. 13 (2022) 4982.
[7] L.E. Gomes, G.M. Morishita, V.E.M. Icassatti, T, et al., ACS Appl. Mater. Interfaces 16 (2024) 117453–117460.
[8] D. Pan, S. Xiao, X. Chen, et al., Environ. Sci. Technol. 53 (2019) 3697–3706.
[9] J. Zhang, S. Lv, J. Zheng, et al., ACS Sustain. Chem. Eng. 8 (2020) 11133–11140.
[10] N. Mano, A. De Poulpiquet, Chem. Rev. 118 (2018) 2392–2468.
[11] B. Xu, Z. Lin, F. Li, et al., Proc. Natl. Acad. Sci. U. S. A. 121 (2024) e2317702121.
[12] D. Wang, L. Chen, X. Feng, Droplet 2 (2023) e51.
[13] L. Yan, B. Xie, C. Yang, et al., Adv. Energy Mater. 13 (2023) 2204245.
[14] H. Furukawa, K.E. Cordova, M. O'Keeffe, O.M. Yaghi, Science 341 (2013) 1230444.
[15] Z. Xie, S. Liang, X. Cai, et al., ACS Appl. Mater. Interfaces 11 (2019) 31671–31680.
[16] X. Ru, H. Chen, Z. Zhang, et al., J. Power Sources 535 (2022) 231411.
[17] X. Sun, J. Chen, J. Zhai, H. Zhang, S. Dong, J. Am. Chem. Soc. 144 (2022) 23073–23080.
[18] C. Ji, J. Hou, K. Wang, Y.H. Ng, V. Chen, Angew. Chem. Int. Ed. 56 (2017) 9762–9766.
[19] B. Wang, S. Lu, Matter 5 (2022) 110–149.
[20] Y. Liu, D. Cheng, B. Wang, et al., Adv. Mater. 36 (2024) 2403775.
[21] Y. Liu, B. Wang, Y. Zhang, et al., Adv. Funct. Mater. 34 (2024) 2401353.
[22] Y. Liu, Z. Ma, G. Yang, et al., Adv. Funct. Mater. 32 (2022) 2109462.
[23] X. Yu, M. Zhou, G. Ren, L. Ma, Chem. Eng. J. 263 (2015) 92–100.
[24] W. Xiong, Y. Peng, W. Ma, et al., Natl. Sci. Rev. 10 (2023) nwad200.
[25] S. Qing, L. Wang, L. Jiang, X. Wu, J. Zhu, SmartMat 3 (2022) 298–310.
[26] P. Xie, C. Chen, C. Zhang, et al., Water Res. 172 (2020) 115475.
[27] S. Chen, M. Yuan, W. Feng, et al., Water Res. 185 (2020) 116220.
[28] K. Liang, C.J. Coghlan, S.G. Bell, C. Doonan, P. Falcaro, Chem. Commun. 52 (2016) 473–476.
[29] K. Liang, J.J. Richardson, J. Cui, et al., Adv. Mater. 28 (2016) 7910–7914.
[30] S. Li, X. Zhou, Z. Chen, et al., ACS Appl. Mater. Interfaces 12 (2020) 11884–11889.
[31] G. Chen, X. Kou, S. Huang, et al., Angew. Chem. Int. Ed. 59 (2020) 2867–2874.
[32] K. Liang, J.J. Richardson, J. Cui, et al., Adv. Mater. 28 (2016) 7910–7914.
[33] N. Zhu, C. Liu, R. Liu, et al., Anal. Chem. 94 (2022) 4821–4830.
[34] W. Liang, P. Wied, F. Carraro, et al., Chem. Rev. 121 (2021) 1077–1129.
[35] Z. Jing, J. Zhan, Adv. Mater. 20 (2008) 4547–4551.
[36] J. Hou, C. Cao, F. Idrees, X. Ma, ACS Nano 9 (2015) 2556–2564.
[37] T. Yimamumaimaiti, X. Lu, J.R. Zhang, L. Wang, J.J. Zhu, ACS Appl. Mater. Interfaces 12 (2020) 41429–41436.
[38] Z. Sun, Y. Wang, L. Zhang, et al., Adv. Funct. Mater. 30 (2020) 1910482.
[39] S. Zeng, F. Lyu, L. Sun, et al., Chem. Mater. 31 (2019) 1646–1654.
[40] J. Tang, X. Yan, W. Huang, et al., Biosens. Bioelectron. 167 (2020) 112500.
[41] Y. Sun, T. Qin, X. Liu, et al., Small 19 (2023) 2206257.
[42] G. Nam, J. Park, M. Choi, et al., ACS Nano 9 (2015) 6493–6501.
[43] T. Lu, Q. Chen, J. Comput. Chem. 43 (2022) 539–555.
[44] X. Zhao, Y.N. Li, G.R. Si, et al., Energy Storage Mater. 68 (2024) 103338.
[45] Y. Pan, H. Xu, M. Chen, et al., ACS Catal. 11 (2021) 5974–5983.
[46] V. Nair, C.L. Perkins, Q. Lin, M. Law, Energy Environ. Sci. 9 (2016) 1412–1429.
[47] Y.S. Chen, L.Y. Lin, Electrochim. Acta 285 (2018) 164–171.
[48] S.N.S. Nasir, N.A. Mohamed, M.A. Tukimon, Physica B Condens. Matter 604 (2021) 412719.
[49] J. Ni, Y. Wen, D. Pan, et al., Chem. Eng. J. 473 (2023) 145162.
[50] X. Bai, W. Liang, J. Sun, et al., J. Environ. Manage. 308 (2022) 114527.
[51] X. Xu, Y. Sun, Z. Fan, et al., Front. Chem. 6 (2018) 64.